Title

Immunotherapeutic Targeting and PET Imaging of DLL3 in Small-Cell Neuroendocrine Prostate Cancer.

Journal

Cancer Research, 83(2)

ISSN

0008-5472

Authors

Chou, Jonathan
Egusa, Emily A
Wang, Sinan
et al.

Publication Date

2023-01-18

DOI

10.1158/0008-5472.can-22-1433

Peer reviewed

HHS Public Access

Author manuscript

Cancer Res. Author manuscript; available in PMC 2023 July 18.

Published in final edited form as:

Cancer Res. 2023 January 18; 83(2): 301–315. doi:10.1158/0008-5472.CAN-22-1433.

Immunotherapeutic targeting and PET imaging of DLL3 in small cell neuroendocrine prostate cancer

Jonathan Chou[1,2,#,*], **Emily A. Egusa**[1,2,3,*], **Sinan Wang**[2,4,15,*], **Michelle L. Badura**[1,2,3,5], **Fei Lee**[6], **Anil P. Bidkar**[4], **Jun Zhu**[1,2,3], **Tanushree Shenoy**[1,2], **Kai Trepka**[1,2,3,7], **Troy M. Robinson**[1,2,3], **Veronica Steri**[1,2], **Jiaoti Huang**[8], **Yuzhuo Wang**[9,10], **Eric J. Small**[1,2], **Emily Chan**[2,11], **Bradley A. Stohr**[2,11], **Alan Ashworth**[1,2], **Brant Delafontaine**[12], **Sylvie Rottey**[12], **Keegan S. Cooke**[13], **Nooshin Hashemi Sadraei**[14], **Brian Yu**[14], **Mark Salvati**[14,16], **Julie M. Bailis**[6], **Felix Y. Feng**[1,2,3], **Robert R. Flavell**[2,4], **Rahul Aggarwal**[1,2,#]

[1]Division of Hematology/Oncology, Department of Medicine, University of California, San Francisco, CA, USA

[2]UCSF Helen Diller Family Comprehensive Cancer Center, San Francisco, CA, USA

[3]Department of Radiation Oncology and Urology, University of California, San Francisco, CA, USA

[4]Department of Radiology and Biomedical Imaging, University of California, San Francisco, CA, USA

[5]Department of Biology, Santa Clara University, Santa Clara, CA, USA.

[6]Oncology Research, Amgen Research, Amgen, South San Francisco, CA, USA

[7]Medical Scientist Training Program, University of California, San Francisco, CA, USA

[8]Department of Pathology, Duke University, Durham, NC, USA

[9]Department of Experimental Therapeutics, BC Cancer, Vancouver, BC, Canada.

[10]Vancouver Prostate Centre, Department of Urologic Sciences, Faculty of Medicine, University of British Columbia, Vancouver, BC, Canada.

[11]Department of Pathology, University of California, San Francisco, CA, USA

[12]Universitair Ziekenhuis Ghent, Ghent, Belgium

[13]Oncology Research, Amgen Research, Amgen, Thousand Oaks, CA, USA

[14]Global Development, Amgen, Thousand Oaks, CA, USA

[15]Present address: School of Biomedical Engineering, ShanghaiTech University, Shanghai, China

[16]Present address: Regeneron Pharmaceuticals, Tarrytown, NY, USA

Abstract

[#]Co-corresponding Authors: Rahul Aggarwal, MD, 1825 Fourth Street, 6th Floor, UCSF Helen Diller Family Comprehensive Cancer Center, San Francisco, CA 94158, Rahul.Aggarwal@ucsf.edu, Ph: 415-353-9278, Jonathan Chou, MD, PhD, 1450 3rd St, Box 3110, UCSF Helen Diller Family Comprehensive Cancer Center, San Francisco, CA 94158, Jonathan.Chou@ucsf.edu, Ph: 415-502-6355.
[*]These authors contributed equally to this work.

Effective treatments for *de novo* and treatment-emergent small cell/neuroendocrine (t-SCNC) prostate cancer represent an unmet need for this disease. Using metastatic biopsies from advanced cancer patients, we demonstrate that delta-like ligand 3 (DLL3) is expressed in *de novo* and t-SCNC and is associated with reduced survival. We develop a positron-emission tomography (PET) agent, [^{89}Zr]-DFO-DLL3-scFv, that detects DLL3 levels in mouse SCNC models. In multiple patient-derived xenograft models, AMG 757 (tarlatamab), a half-life-extended bispecific T cell engager (BiTE®) immunotherapy that redirects CD3-positive T cells to kill DLL3-expressing cells, exhibited potent and durable anti-tumor activity. Late relapsing tumors after AMG 757 treatment exhibited lower DLL3 levels, suggesting antigen loss as a resistance mechanism, particularly in tumors with heterogeneous DLL3 expression. These findings have been translated into an ongoing clinical trial of AMG 757 in *de novo* and t-SCNC, with a confirmed objective partial response in a patient with histologically confirmed SCNC. Overall, these results identify DLL3 as a therapeutic target in SCNC and demonstrate that DLL3-targeted BiTE® immunotherapy has significant anti-tumor activity in this aggressive prostate cancer subtype.

Keywords

small cell/neuroendocrine prostate cancer; bispecific T cell engager; delta like ligand 3 (DLL3); positron emission tomography (PET); patient derived xenograft (PDX); clinical trial

INTRODUCTION:

Advanced small cell/neuroendocrine prostate cancer (SCNC) is an invariably fatal disease, and can arise *de novo* or after prolonged exposure to androgen deprivation therapy, commonly referred to as treatment-emergent SCNC (t-SCNC) (1). Treatment choices beyond first-line platinum-based chemotherapy are limited and response rates are modest (2,3). Delta-like ligand 3 (DLL3) is a Notch ligand that is highly expressed during embryonic development in the spinal cord and nervous system (4–6). Although the function of DLL3 remains poorly understood, it is implicated in inhibiting the Notch signaling pathway, a key regulator of cell fate decisions (7). DLL3 is expressed in multiple neuroendocrine (NE) carcinomas, but not in most normal adult tissues, making it an attractive NE carcinoma surface protein target.

Prior efforts to target DLL3 in NE carcinomas have been disappointing. The first-in-class antibody-drug conjugate (ADC), Rovalpituzumab tesirine (Rova-T), targeted DLL3 to deliver the DNA intercalating agent pyrrolobenzodiazepine (PBD) to tumor cells. In small cell lung cancer (SCLC) and large cell NE models, Rova-T significantly inhibited tumor growth compared with standard chemotherapy (8). The phase I study in patients with recurrent SCLC (NCT01901653) showed encouraging results, but subsequent studies with various NE carcinomas demonstrated only modest objective response rates, with high incidence of adverse events including pleural effusions, pericardial effusions and peripheral edema, which halted further clinical development (9–15). The toxicity was attributed to the release of PBD from the ADC linker (16). DLL3 therefore remains a therapeutic target of high interest in NE carcinomas, including prostate SCNC (11,17,18).

AMG 757 (tarlatamab) is a DLL3-targeted immune therapy with a distinct mechanism of action from Rova-T. AMG 757, a half-life extended bispecific T cell engager (HLE BiTE®) molecule (19), is designed to redirect a patient's T cells to kill DLL3-expressing tumor cells (20). AMG 757 activity was previously demonstrated in cell lines and patient-derived xenograft (PDX) models of SCLC (20). Toxicology studies in cynomolgus monkeys showed that AMG 757 had favorable safety and pharmacokinetic profiles (20). AMG 757 subsequently advanced into clinical trials, and results from the phase 1 study in SCLC patients demonstrated preliminary evidence for efficacy and an acceptable safety profile (21,22).

Here, we interrogate DLL3 expression in metastatic prostate cancer biopsies, and show that DLL3 is enriched in *de novo* and t-SCNC. We provide proof-of-concept for therapeutic imaging of DLL3-expressing tumors with a sensitive and specific DLL3 PET radiotracer. We present the first preclinical evidence for AMG 757 activity in PDX models of prostate SCNC, including a t-SCNC PDX model (23), and investigate mechanisms of BiTE® response and resistance. Finally, we present the first confirmed objective radiographic response to AMG 757 in a prostate cancer patient with SCNC.

MATERIALS AND METHODS:

Patient studies.

Patients with metastatic castration resistant prostate cancer (mCRPC) who gave written informed consent underwent a metastatic tumor biopsy using methods as previously described (24). The first biopsy was fresh frozen, and underwent laser capture microdissection and subsequent RNA-sequencing as previously described (24). The second biopsy core from the same metastatic lesion was formalin-fixed, paraffin-embedded, and underwent hematoxylin and eosin (H&E) staining and immunostaining for DLL3 (Ventana clone SP347). An expert prostate cancer pathologist (JH) determined the histological classification of the biopsy (t-SCNC versus adenocarcinoma) using established morphologic criteria. Two other expert pathologists (BAS and EC) blinded to clinical outcomes and histologic classification reported the histo (H)-score of DLL3 expression for each evaluable biopsy sample. Subsequent to metastatic biopsy, patients were prospectively followed for survival outcomes.

Animal studies.

All studies followed the guidelines of the Association for Assessment and Accreditation of Laboratory Animal Care and performed under an approved Institutional Animal and Use Committee (IACUC) protocol (AN182067). Briefly, 8–10 week old male NSG (NOD/SCID/gamma) mice were implanted with small pieces of prostate cancer patient-derived xenograft (PDX) tumors obtained from Living Tumor Lab (www.livingtumorlab.com) (25) or injected with 5×10^6 NCI-H660 cells. When tumors reached a size between 50–100 mm^3, mice were randomized into control and treatment groups. On day 0, 20×10^6 CD3+ or CD8+ activated T cells were injected intravenously (IV) through the tail vein. On day 1, NT control BiTE® molecule (EGFRvIII HLE BITE®) or AMG 757 was injected IV at indicated doses, ranging from 0.3 to 3 mg/kg, as previously described (20). Additional BiTE® injections were

administered IV weekly on days 8 and 15. Tumor dimensions were measured bi-weekly with calipers and volume was calculated according to the formula $V=0.52*length*width^2$, where the width represents the shorter axis. Mice were humanely euthanized once the tumor volume reached 2000 mm^3. For the NCI-H660 experiment, tumors were harvested on day 45 for either T cell phenotyping by flow cytometry (left flank tumor) or immunohistochemistry (right flank tumor). For flow cytometry, tumors were collected and dissociated for analysis of tumor-infiltrating T cells. NCI-H660 tumors were minced and placed in Liberase TL (0.2 mg/mL; Roche) with DNase I (20 units/mL; Ambion), and then the cell suspensions were homogenized with a gentleMACS Dissociator (Miltenyi Biotech) and incubated at 37°C for 15 minutes on a MACSmix Tube rotator (Miltenyi Biotech). Cells treated with 0.02% EDTA (Sigma) and heat-inactivated FBS (Thermo Fisher), were filtered and centrifuged, and then washed with staining buffer and incubated with antibodies to human T cell markers (see Supplemental Material). Cells were analyzed by flow cytometry on a LSR Fortessa (Becton Dickinson) and FlowJo software, version 10 (FlowJo). For the PDX experiments, tumor tissues were collected for histology by preservation overnight at 4°C in 10% neutral buffered formalin and changed to 70% ethanol 24-hours later. Tissue was paraffin-embedded and processed for histology. Additional tissue was also snap-frozen for downstream applications.

Histology and immunostaining.

Routine histochemical and immunohistochemical stains were used to characterize tumors. Tumors were fixed in 10% neutral-buffered formalin for 24 hours and processed to paraffin blocks. Serial histologic sections were stained for H&E or used in IHC assays, which were performed using a Discovery Ultra Stainer (Ventana Medical Systems) using reagents designed for Ventana instruments and antibodies directed against human DLL3 (Ventana SP347), CD4 or CD8 (Spring Biosciences or Cell Signaling Technology), and PD-1 or an isotype control antibody (Abcam). Antigen retrieval was performed on deparaffinized tissue using the BioSB TintoRetriever and either citrate or EDTA buffer based on the antibody manufacturer's recommendations. Slides were incubated with the primary antibody or isotype control for 1 hour at room temperature and with OmniMap HRP secondary antibodies (Roche Diagnostics) for 15 minutes at room temperature. Complexes were detected using a Ventana DAB chromogen kit (Roche Diagnostics), and sections were counterstained with hematoxylin. Analysis of histologic sections was performed using a Nikon Eclipse 90i microscope, scanned using an Aperio scanner (Leica) and processed using ImageJ software. Archival FFPE human lymph node samples were used as a positive control for CD4, CD8 and PD-1 immunostaining.

Tumor Dissociation:

PDX tumors were cut into small pieces and enzymatically digested with Collagenase III (Worthington, 5 U/mL) and DNase I (Sigma, 20 U/mL) in DMEM High Glucose medium (Thermo Fisher) using gentleMACS™ Octo Dissociator or the Tumor Dissociation Kit (Miltenyi Biotec). Tumor tissue was homogenized and enzymatically digested as above. After digestion, cells were passed through a 70 μm filter followed by a 40 μm filter and washed with wash medium (DMEM/F12 + 10% FBS + 1% Antibiotic-Antimycotic). The cells were resuspended in culture medium (RPMI GlutaMAX+ 5% FBS+ 1x Insulin-Transferrin-Selenium (ITS-G) + 10 nM Hydrocortisone+ 10 nM beta-estradiol+

1x GlutaMAX+ 1x Antibiotic-Antimycotic). Human tumor cells were enriched using the Mouse Cell Depletion Kit (Miltenyi Biotec) and resuspended in culture medium.

Flow cytometry:

Tumor cells were stained with either 1 ug/mL of AMG 757 or NT control BiTE® molecule (Amgen) followed by incubation with goat anti-human IgG (H+L) cross-adsorbed secondary antibody Alexa Fluor 647 (Thermo Fisher). Cells were analyzed on a FACSymphony™ (BD Biosciences) or Attune NxT (Thermo Fisher), and data were analyzed with FlowJo software (BD Biosciences).

T cell isolation and expansion.

Human T cells were isolated from a Leukopak (Stemcell Technologies) using the EasySep Human CD8+ T Cell Isolation Kit and grown in Immunocult medium (Stemcell Technologies) at 37°C. On the day of isolation, cells were activated by CD3/CD28 Dynabeads and supplemented with 50 IU/ml interleukin-2 (IL2; Stemcell Technologies). Cells were split every 2–3 days to 1×10^6/ml and supplemented with IL2 at each split until 13 days post-isolation. Activated T cells were frozen at −80°C and thawed on the day of injection into mice. Activation and immunotyping of T cells was verified by flow cytometry using fluorescently-labeled antibodies to CD25, CD69, CD45, CD3, CD4, and CD8 (BD Biosciences).

In vitro cytotoxicity assays:

Dissociated tumor cells (target cells) were co-cultured with human T cells (effector cells) at an effector-to-target (E:T) cell ratio of 10:1 in the presence of HLE BiTE® molecules. After a 48h incubation, cells were analyzed for T cell-dependent cellular cytotoxicity (TDCC), T-cell activation and cytokine production. Tumor cell viability was assessed by flow cytometry using an antibody to human EpCAM (Biolegend) or TO-PRO-3 Iodide (Thermo Fisher) to identify dead cells. T-cell activation was assessed by flow cytometry using antibodies to CD25 and CD69 (BD Biosciences). Cells were incubated with antibodies for 30 minutes at 4°C, washed in FACS buffer and analyzed on a FACSymphony™ (BD Biosciences). Cytokines in the supernatants were quantified using the Human ProInflammatory Culture Kit (K15009B) on MESO Sector S600 (Meso Scale Discovery) according to the manufacturer's instructions.

Western blotting.

Cells were lysed in RIPA buffer with added Halt protease and phosphatase inhibitor (Thermo Fisher) and protein concentration was measured using the BCA Protein Assay Kit (Thermo Fisher). Lysates were combined with 4x NuPAGE LDS (Thermo Fisher) loading buffer supplemented with 5% beta-mercaptoethanol. Samples were subjected to SDS-PAGE and polyacrylamide gels were transferred to PVDF membranes, blocked in 5% w/v BSA, and incubated with primary antibody overnight at 4°C. The next day, horseradish peroxidase-conjugated (HRP) secondary antibodies were added and the blot was visualized using ECL Detection Reagents (Genesee Scientific). The following antibodies were used at the indicated concentrations: DLL3 (Cell Signaling Technology #71804S, 1:1000), V5

(Cell Signaling Technology #13202, 1:1000), GAPDH (Cell Signaling Technology #2118S, 1:8000), anti-rabbit IgG, HRP-linked (Cell Signaling Technology #7074, 1:7000).

Cell culture.

SHP-77 SCLC and 22Rv1 prostate cancer cells were obtained from the American Type Culture Collection (ATCC). C42B cells were obtained from the University of Michigan. Cells were grown in standard RPMI media (Life Technologies) supplemented with 10% FBS (Seradigm) and penicillin/streptomycin. Cells were routinely tested for mycoplasma (last tested December 2021, MycoAlert Lonza) and validated by STR DNA profiling (Genetica). All experiments were conducted within 20 passages from the parental stock.

Cloning DLL3 and generation of stable cell lines.

The DLL3 cDNA (Dharmacon) was cloned using the Gateway recombination system into a lentiviral vector (pLV-Blasticidin) with an N-terminus V5 epitope tag to facilitate detection. Lentiviral production was carried out using calcium-phosphate-mediated transfection of HEK293T-Lenti-X cells and collected between 48–96 hours. Lentivirus was concentrated using the Lenti-X Concentrator (Takara) according to manufacturer's instructions. To generate the stable lines, cells were transduced with lentivirus and selected with blasticidin (3–5ug/ml) for at least 5 days.

IncuCyte co-culture assays.

SHP-77, 22Rv1 or C42B cancer cells well labeled with NucLightGreen or NucLightRed (Sartorius) as indicated. On day 0, 3–5 $\times 10^3$ cells were plated and left overnight to attach. On day 1, cells were treated with NT control BiTE® (5 nM), AMG 757 (5 nM), or AMG 160 (400 pM), and co-cultured with activated T cells, which were plated at an effector-to-target ratio of 5:1 or 10:1. The plates were loaded into an IncuCyte S3 Live Cell Analysis System (Sartorius), and images were obtained every 4–6 hours over 5 days.

Conjugation of p-Isothiocyanate-benzyl-DFO to scFv.

An anti-DLL3 scFv that bound the epidermal growth factor (EGF) domain of human, non-human primate and mouse DLL3 was identified by phage display and used to generate a DLL3 PET tracer. To perform the conjugation, 2 mg anti-DLL3 scFv (Amgen) was exchanged to 0.1 mol/L Na_2CO_3-$NaHCO_3$ buffer, pH 9, using a 30K MW centrifugal filter. The final volume was adjusted to 0.4 mL by adding 0.1 mol/L Na_2CO_3-$NaHCO_3$ buffer, pH 9. p-Isothiocyanate-benzyl-DFO (1.2 mg, Macrocyclics, catalog B-705) was dissolved in 57.5 μL DMSO. p-Isothiocyanate-benzyl-DFO solution (8 μL; 3 equivalents to scFv) was added to the 0.4 mL solution containing 2 mg of scFv. The mixture was incubated at 37°C for 45 minutes. The mixture was purified with a PD10 gel filtration column by eluting with 0.25 mol/L sodium acetate solution, pH 6. All chemicals were from Sigma-Aldrich, Inc.

Radiolabeling.

4μL (1.2 mCi) ^{89}Zr oxalate (from 3D Imaging and the Cyclotron Laboratory at University of Wisconsin, Madison), 4 μL 1 mol/L Na_2CO_3, 200 μL 1 mol/L NH_4OAc, and 40 μg DFO-scFv were incubated at room temperature for 0.5 hour. The mixture was subject to

instant thin layer chromatography (iTLC) to determine labeling yield, and then purified with a PD10 column by eluting with 0.9% normal saline. The final product was also analyzed for purity by iTLC. iTLC-SG (catalog No. SG10001) was purchased from Agilent Technologies.

In vitro K_d measurement.

1 μg/mL recombinant DLL3 (ACROBiosystems, DL3-H52H4) in PBS was placed in a 96-well Nunc MaxiSorp Plate (100 μL/well, Invitrogen) and kept at 4°C for 24 hours before testing (in triplicate). The buffer was removed, and then the wells were washed with PBS two times. PBS with 1% nonfat milk was added to each well and incubated for 1 hour to minimize subsequent nonspecific protein binding. The buffer was removed and various concentrations (100 μL/well, 0.0005–50 nmol/L) of [^{89}Zr]DFO-scFv in PBS were added, and incubated for 1 hour at room temperature. Bound radioactivity was quantified and analyzed as previously described (26).

DLL3 magnetic beads target binding fraction assay.

HisPur Ni-NTA Magnetic Beads (catalog No. 88831) were prepared as previously described (26). PBST (380 μL) and 20 μL of 100 μg/mL DLL3 were added to the beads and incubated for 15 minutes. The supernatant was removed, and the beads were washed with 400 μl PBST once. [^{89}Zr]DFO-scFv (2.7 ng) in 1% milk PBS was added to each vial of group A and B. 20 μg scFv was added to each vial of the blocking group B. Samples were diluted to 400 μL per vial using 1% milk PBS, incubated for 30 minutes, and washed with 1% milk PBS twice. The activity of beads and 2.7 ng [^{89}Zr]DFO-scFv was read using a Hidex Gamma Counter. Binding percentage was calculated by beads activity/2.7 ng [^{89}Zr]DFO-scFv activity.

In vivo [^{89}Zr]DFO-scFv PET imaging and biodistribution studies.

Mice with tumors reaching 300–500 mm^3 were anesthetized by isoflurane inhalation. 1.48–1.85 MBq (40–50 μCi, 2 μg/mouse) of [^{89}Zr]DFO-scFv in saline was administered through tail vein injection. The animals were imaged at various timepoints with a 20-minute acquisition time by using microPET/CT (Inveon, Siemens Medical Solutions). Following completion of the experiments, the animals were euthanized, major organs harvested, weighed, and the radioactivity measured in a Hidex gamma counter. Analysis of images and biodistribution data was conducted as previously described (26).

Statistical analysis.

Data were analyzed using the unpaired, two-tailed Student t test and one-way ANOVA. Differences at the 95% confidence level ($P < 0.05$) were considered to be statistically significant. Multiple correction testing was used as appropriate (GraphPad Prism). For the patient studies, a log-rank test was used to compare the overall survival from the date of biopsy of patients with absent versus positive DLL3 immunohistochemical expression on metastatic biopsy. The correlation between *DLL3*, *STEAP1*, and *FOLH1 (PSMA)* expression on RNA-seq was evaluated using Spearman's rank correlation method.

Study approval.

All animal work was performed in accordance with UCSF Preclinical Therapeutics Core or Amgen Institutional Animal Care and Use Committee (IACUC) approved protocols. For biopsy samples, patients with metastatic castration resistant prostate cancer (mCRPC) gave written informed consent on the PROMOTE biopsy clinical trial (NCT02735252) prior to a metastatic tumor biopsy as previously described (24). The patient cited on the clinical trial of AMG 757 in neuroendocrine prostate cancer (NCT04702737) gave written informed consent prior to initiation study treatment, in accordance with recognized ethical guidelines as described by the Declaration of Helsinki and U.S. Common Rule.

Data availability:

Data described within the manuscript are available upon request from the corresponding authors, with the exception of all patient data information, which are subject to approval due to patient privacy.

RESULTS:

DLL3 is expressed in metastatic prostate cancer biopsies

To assess DLL3 expression in patients with metastatic castration-resistant prostate cancer (mCRPC), we collected biopsy samples from multiple metastatic sites including bone, liver and lymph nodes. Twenty-four biopsies were evaluable for DLL3 expression. Twelve of 24 (50%) samples were classified histologically as *de novo* or t-SCNC, and 12/24 (50%) were classified as adenocarcinoma. Of the 12 mCRPC biopsies with *de novo* or t-SCNC, 9 (75%) were positive for DLL3 expression by immunohistochemistry (IHC), with range of H-scores from 5–280 (mean H-score = 43) consistent with prior studies (17) (Fig. 1a–1b). In contrast, DLL3 was not expressed in any of the adenocarcinoma samples (Mann-Whitney p-value = 0.0003) (Fig. 1a). DLL3 expression on mCRPC biopsy was associated with shortened survival (hazard ratio = 4.46 (95% CI: 1.27 – 15.7), log-rank p-value = 0.0201) (Fig. 1c). Using prior gene expression datasets, we found a negative correlation between *DLL3* and both *STEAP1* and *FOLH1* (the gene encoding PSMA), and confirmed high *DLL3* in the SCNC samples (Supp Fig. 1) (24,27). Taken together, these results demonstrate that *de novo* and t-SCNC samples from metastatic sites express DLL3, validating DLL3 as an important therapeutic target.

The DLL3-targeted HLE BiTE® AMG 757 promotes T-cell killing of tumor cells *in vitro*

To determine whether DLL3 expression is sufficient for AMG 757-mediated killing of prostate cancer cells, we overexpressed V5-tagged DLL3, or LacZ as a control, in 22Rv1 prostate adenocarcinoma cells, which do not express endogenous DLL3 (Fig. 2a–2b). SHP-77, a SCLC cell line which expresses endogenous DLL3, was used as a positive control. Overexpression of DLL3 did not change cell morphology (Supp. Fig. 2a) or affect cell proliferation (Fig. 2c). We incubated the control and DLL3-expressing 22Rv1 prostate cancer cells with T cells at an effector-to-target (E:T) ratio of 5:1, and added either a non-targeting (NT) control BiTE® molecule or AMG 757. We found that the DLL3-expressing 22Rv1 cells were robustly killed by AMG 757 (Fig. 2c, Supplemental Movies 1a–1d). In

contrast, 22Rv1 cells that did not express DLL3 continued to proliferate when treated with either AMG 757 or the NT control BiTE® molecule (Fig. 2c, Supplemental Movies 1a–1d). Similar results were obtained in a second prostate adenocarcinoma cell line (C42B), where we exogenously expressed DLL3 (Supp. Fig. 2b–2c). AMG 757-mediated cell death is therefore specific for tumor cells that express DLL3.

AMG 757 is designed to induce T cell activation and expansion, cytokine production, and redirected T cell lysis. In co-cultures of human T cells with DLL3-positive NCI-H660 prostate SCNC cells, we found that AMG 757, but not a NT control BiTE® molecule, induced activation of both CD4+ and CD8+ T cells, as marked by CD69+ staining (Fig. 2d), secretion of IFNγ and TNFα cytokines (Fig. 2e–2f), and T cell dependent cytotoxicity (Fig. 2g). These results demonstrate that AMG 757 robustly activates T cells and induces killing of DLL3-expressing prostate cancer cells.

DLL3 expression in patient-derived xenograft (PDX) models of prostate cancer

To identify relevant *in vivo* prostate cancer SCNC models with DLL3 expression, we analyzed PDX models from the Living Tumor Lab (25). We found that adenocarcinoma models had high mRNA levels of *FOLH1* and androgen receptor (*AR*) but little to no *DLL3* expression. In contrast, the SCNC models had high *DLL3* with minimal expression of *FOLH1* or *AR* mRNA (Fig. 3a). We then demonstrated that the DLL3 protein was expressed in these models and present on the cell surface (Fig. 3b–3c). Importantly, we identified PDX SCNC models with low and high DLL3 expression and with homogeneous and heterogeneous staining patterns. The LTL-331R (H-score of 180) and LTL-545 (H-score of 280) models, which showed different DLL3 expression levels, were selected for subsequent studies.

To extend our findings of AMG 757-mediated tumor killing to the PDX lines, we dissociated tumor cells from the LTL-331R PDX and confirmed DLL3 surface protein expression by flow cytometry (Fig. 3d). We then incubated the tumor cells with human T cells and either AMG 757 or a NT control BiTE® molecule *ex vivo*. We found that AMG 757 induced IFNγ and TNFα secretion (Fig. 3e–3f), as well as T cell activation, expansion and T cell-dependent cytotoxicity (Fig. 3g–3i), while the NT control BiTE® did not. We also evaluated AMG 757 activity in LTL-545 PDX dissociated tumor cells (Supp. Fig. 3a–3c). These results demonstrate that AMG 757 induces tumor cell death in prostate PDX models of SCNC.

Detection of DLL3-expressing tumors with a DLL3 immuno-PET tracer

We used the DLL3-binding single-chain variable fragment (scFv) from our first-generation DLL3-targeted BiTE molecule (19) to generate a PET tracer for a proof-of-concept imaging study. Like AMG 757, the DLL3-binding scFv cross-reacts to human, mouse and cynomolgus monkey DLL3, and does not cross-react with related family members DLL1 or DLL4. We performed a two-step procedure for ^{89}Zr labeling by first conjugating the scFv with deferoxamine (DFO) followed by chelation of the ^{89}Zr to produce the final product [^{89}Zr]DFO-DLL3 (Fig. 4a). MALDI spectrometry showed an average of 0.3 copies of the chelator per scFv (Supp. Fig. 4a–4b). The ^{89}Zr labeling yield was 95.5 ± 3.3% (n = 8). After

size exclusion chromatography purification, the radiopharmaceutical purity was consistently >98% (Fig. 4b). The specific activity ranged from 999–1110 MBq/mg (n = 10, 26.7–29.6 GBq/μmol, 27–30 mCi/mg, 720.9–801 mCi/μmol). The Kd of the [^{89}Zr]DFO-DLL3-scFv probe was determined by a saturation binding assay (Kd 50.3 ± 2.0 nM) (Supp. Fig. 5). A magnetic bead-based radioligand binding assay (28) was then used to determine the target binding fraction of the labeled [^{89}Zr]DFO-DLL3-scFv of 89.4% ± 2.1%. The binding was reduced to 45.3% ± 2.4% by adding excess cold scFv to the [^{89}Zr]DFO-DLL3-scFv at the time of the assay (Fig. 4c). These data demonstrate that [^{89}Zr]DFO-DLL3-scFv can be radiolabeled in a reproducible, high-yield manner without significant loss of binding activity.

To evaluate the capability of [^{89}Zr]DFO-DLL3-scFv to detect DLL3-expressing tumors *in vivo*, we implanted 22Rv1 cells expressing either DLL3 or LacZ (control) into contralateral flanks. Mice with dual xenograft tumors were administered a single dose of [^{89}Zr]DFO-DLL3-scFv and imaged at 2h, 4h and 24h post-injection. Tumor and tissue samples were then analyzed for radiotracer uptake. Biodistribution analysis showed that the uptake of the PET tracer in 22Rv1-DLL3 tumor cells was 1.28 ± 0.24%ID/g at 2h post-injection, 1.38 ± 0.17% ID/g at 4h post-injection, and 1.48 ± 0.47%ID/g at 24 h post-injection, suggesting fast tumor uptake and a long retention time. In contrast, minimal uptake was observed in the 22Rv1-LacZ tumor (0.53 ± 0.05%ID/g at 24h post injection). (Fig. 4d–4e and Supp. Table S1). Because of the steady uptake in tumor and fast clearance in blood and muscle, the tumor/muscle and tumor/blood ratios increased over time (tumor:muscle ratio 8.33 ± 2.43 in 22Rv1-DLL3 tumors and 3.17 ± 1.20 in 22Rv1-LacZ tumors; tumor:blood ratio 4.60 ± 1.17 in 22Rv1-DLL3 tumors and 1.68 ± 0.24 in 22Rv1-LacZ tumors at 24h) (Fig. 4f). As expected for an scFv-based PET agent, the tracer demonstrated high uptake in the kidney (29). These data demonstrate that [^{89}Zr]DFO-DLL3-scFv effectively detects DLL3-expressing tumor cells *in vivo*.

Comparison of PET imaging and biodistribution of [^{89}Zr]DFO-DLL3-scFv in clinically relevant PDX models of prostate SCNC

We next used PET imaging with [^{89}Zr]DFO-DLL3-scFv as a noninvasive biomarker to measure DLL3 levels in our PDX models with varying endogenous expression levels of DLL3. Mice with LTL-545 tumors (a DLL3^{HI} model) were injected with [^{89}Zr]DFO-DLL3-scFv and were imaged at 2h, 4h and 24h. To test the probe specificity, imaging was performed by co-injecting [^{89}Zr]DFO-DLL3-scFv with 200-fold excess of cold DLL3-scFv (Supp. Fig S6). Indeed, we found high uptake of [^{89}Zr]DFO-DLL3-scFv in the LTL-545 xenografts (Fig. 5a, Supp. Fig. S6 and Table S2). The tumor/blood and tumor/muscle ratios increased from 0.39 ± 0.04 at 2h to 3.29 ± 0.77 at 24h and from 3.26 ± 0.86 at 2h to 10.85 ± 1.37 at 24h (Fig. 5b), and uptake was effectively blocked by cold DLL3-scFv. In contrast, [^{89}Zr]DFO-DLL3-scFv uptake was lower in the LTL-331R model (DLL3^{LOW}) and minimal in the LTL-484 model (DLL3^{NEG}) (Fig. 5c–5d, Supp. Fig. S7a–7b and Supp. Table S3). These data support the feasibility of using [^{89}Zr]DFO-DLL3-scFv as a radiotracer for PET imaging, which could serve as a noninvasive biomarker of DLL3 expression *in vivo*.

In vivo efficacy of AMG 757 in prostate SCNC models

We next performed experiments in our SCNC PDX models to assess AMG 757 antitumor efficacy. We first utilized LTL-545, a $DLL3^{HI}$ model. We administered activated, non-HLA matched human T cells on Day 0, followed by weekly injections of AMG 757 starting on Day 1 (Supp. Fig. S8a). AMG 757 dramatically suppressed PDX tumor growth (2,215 ± 171 mm^3 vs 192 ± 81 mm^3, $p<0.0001$, Fig. 6a–6b) and significantly prolonged overall survival (OS; median OS 34 vs 76 days, HR=0.23, log-rank p value = 0.0002) (Fig. 6c). Robust CD8+ T cell infiltration occurred in the tumors of mice treated with T cells plus AMG 757 but not in mice that received T cells plus the NT control BiTE® molecule (Fig. 6d). Interestingly, 4 of 20 mice (20%) had complete responses (CRs) that were durable through the end of the study (90 days after the first AMG 757 treatment), suggesting that AMG 757 can induce long-term responses.

We wondered whether AMG 757 would have similar efficacy in the LTL-331R, a $DLL3^{LOW}$ model. This model, which was derived after castration and is one of the only models that represents t-SCNC (23), and has lower, more heterogeneous levels of DLL3 expression than the LTL-545 ($DLL3^{HI}$) model (Fig. 3b–3c). We found that AMG 757 also suppressed tumor growth (1,785 ± 167 mm^3 vs 715 ± 166 mm^3, $p<0.001$) and extended OS (median OS 44 vs 67 days, HR=0.31, log-rank p value = 0.0006) (Fig. 6e–6f). Furthermore, AMG 757 suppressed tumor growth in a third PDX model (LTL-370) (Supp. Fig. S8b–8c) and in the NCI-H660 xenograft model, which both express high levels of DLL3 (Supp. Fig. S9a). Anti-tumor efficacy was associated with increased T cell infiltration and activation in the tumors (Supp. Fig. S9b–9e). Taken together, our data demonstrate that AMG 757 has potent activity and can achieve durable responses in a broad range of *de novo* and t-SCNC models.

Loss of DLL3 is a potential resistance mechanism to AMG 757

Our observation that AMG 757 tumor growth control was more durable in the $DLL3^{HI}$ PDX models than in the LTL-331R t-SCNC model led us to investigate mechanisms of resistance. The LTL-331R model has low, heterogeneous expression of DLL3, suggesting that individual cells with minimal or no expression of DLL3 might not respond to AMG 757 treatment. AMG 757 treatment initially suppressed LTL-331R tumor growth, but most tumors eventually relapsed. Interestingly, there was an early relapse (ER) group and a late relapse (LR) group (Fig. 7a). We found that total DLL3 levels were similar between the NT control BiTE® molecule-treated and AMG 757-treated, ER group at the study endpoint. This suggested that the ER tumors did not result from outgrowth of DLL3-negative tumor cells. However, DLL3 expression was markedly lower in the AMG 757-treated, LR group as compared to the other groups (Fig. 7b). IHC analysis also demonstrated lower, more heterogeneous DLL3 cell surface expression in the LR group (Fig. 7c), and lower levels of *DLL3* mRNA, suggesting these changes may be occurring through a transcriptional mechanism (Fig. 7d). We did not find differences in DLL3 expression in the $DLL3^{HI}$ LTL-545 tumors that escaped AMG 757 (data not shown). Together these data suggest that downregulation or loss of DLL3 expression is a potential mechanism of resistance to AMG 757. However, our finding that DLL3 expression is maintained in LTL-331R tumors that relapse early, and in $DLL3^{HI}$ LTL-545 tumors suggests that there are additional mechanisms of resistance that are independent of target antigen expression.

To further study the impact of DLL3 target heterogeneity on AMG 757 antitumor response, we developed an *in vitro* system to test bystander killing of DLL3-negative cells. We labeled 22RV1 cells (which do not express endogenous DLL3) with NucLightGreen and SHP-77 cells (which do express endogenous DLL3) with NucLightRed and co-cultured these two populations together (Supp. Movies 2a–c). We then added AMG 757 or the NT control BiTE® molecule with T cells. As expected, the SHP-77 DLL3-expressing cells were killed by AMG 757 but not by the NT control BiTE®. This killing was robust, even in the presence of DLL3-negative 22RV1 cells. However, 22RV1 cells co- cultured with SHP-77 cells were not killed by AMG 757 treatment (Fig. 7e), suggesting that there was minimal bystander T cell killing. As a control, we showed that the 22RV1 cells, which express endogenous PSMA, were appropriately targeted when incubated with the PSMA-targeting BiTE® molecule AMG 160 (Supp. Fig S10a). We also performed co-culture experiments with green 22RV1 control and red 22RV1-DLL3 cells and found similar results, with AMG 757 selectively targeting the DLL3-expressing cells (Supp. Fig S10b). Taken together with the *in vivo* studies described above, our data suggest that AMG 757 has antitumor activity even against tumor cells with low or heterogeneous DLL3 expression, shows limited bystander killing, and that downregulation or loss of DLL3 expression is one potential mechanism that allows for tumor cells to escape AMG 757-mediated cell death.

Objective response to AMG 757 in a patient with t-SCNC

Our pre-clinical findings, together with emerging clinical data for AMG 757 in SCLC, led us to test AMG 757 in patients with *de novo* and t-SCNC prostate cancer (NCT04702737). The first confirmed objective response observed on study was achieved in a patient with *de novo* SCNC prostate cancer comprising approximately 50% of the primary tumor specimen. This patient, a 70-year old man, had a prostatectomy and was treated with androgen deprivation therapy. He was then treated with radiation therapy and platinum/etoposide chemotherapy, which was discontinued after 5 cycles due to toxicity. The patient subsequently developed a new soft tissue mass at the junction of the right ureter and iliac vessels (Fig. 8a), causing right sided hydronephrosis, and the patient was enrolled on the AMG 757 study. Serum PSA levels were normal at diagnosis and throughout his treatment course. Baseline serum neuroendocrine markers including neuron-specific enolase (NSE) and chromogranin A were within normal limits, and the patient was treated with AMG 757 every two weeks. Adverse events including grade 1 cytokine release syndrome (CRS), dyspepsia and constipation occurred during the first cycle of treatment. A computed tomography (CT) scan performed after seven weeks of treatment showed a decrease in the tumor size and near resolution of the hydronephrosis. A subsequent CT scan done at 15 weeks after the initiation of AMG 757 showed further decrease of the tumor resulting in a partial response (PR) according to RECIST criteria (Fig. 8b). The patient has remained on treatment for 10 months with an ongoing confirmed PR. The primary tumor sample showed 70% positivity for DLL3 by IHC, with an H-score of 125. Altogether, this case highlights the potential for AMG 757 to benefit SCNC prostate cancer patients.

DISCUSSION:

Both *de novo* and t-SCNC are aggressive diseases that are currently not curable. Using biopsies taken from mCRPC patients, we validate DLL3 as a cell surface marker that is specifically expressed in small cell/neuroendocrine prostate cancer, and not expressed in prostate adenocarcinoma. DLL3 expression is associated with shortened survival outcomes underscoring the high unmet medical need in this patient population. Our data confirm initial reports of DLL3 expression and validate DLL3 as a relevant therapeutic target in *de novo* and t-SCNC prostate cancer. Using a combination of cell line and PDX models, we demonstrate that targeted immunotherapy with AMG 757 can effectively activate cytotoxic T cells and durably suppress tumor growth with a finite course of treatment. Similar preclinical efficacy was observed for AMG 757 in SCLC models (20) and early clinical data showed encouraging efficacy of AMG 757, with an overall response rate of 23% of SCLC patients and a median duration of response of 13.0 months (21,22). We now demonstrate encouraging preliminary clinical activity of AMG 757 in SCNC prostate cancer, with a confirmed objective response in a patient previously treated with androgen deprivation therapy and platinum-based chemotherapy. DLL3 therefore remains an important therapeutic target, given its expression in 75% of mCRPC metastatic biopsies with t-SCNC histology.

Expression of the surface target antigen is one critical factor mediating sensitivity to BiTE® molecules (19). Indeed, we demonstrate that in co-cultures with CD3+ T cells, exogenous DLL3 expression in prostate adenocarcinoma cells is sufficient for AMG 757 activity. Tumor models with low levels of DLL3 expression were sensitive to AMG 757, although decreased or heterogeneous tumor DLL3 expression may be a potential resistance mechanism. Whether this is due to downregulation of DLL3, or due to preferential outgrowth of $DLL3^{NEG}$ tumor cells is not well understood. ASCL1, a key regulator of DLL3 expression, is one of the most highly up-regulated transcription factors in *de novo* and t-SCNC (30) and defines a subtype of SCLC (31). While the regulatory mechanisms underlying DLL3 expression beyond ASCL1 are not well understood (32), one possibility is that the lineage plasticity of tumors with neuroendocrine characteristics may affect DLL3 expression levels. Future work to systemically identify and characterize these pathways in prostate cancer cells will be critical for developing strategies to increase AMG 757 efficacy and prevent resistance.

Our data also demonstrate that regrowth of DLL3-positive tumors can occur, suggesting that additional factors may impact BiTE®-mediated anti-tumor responses. Indeed, while there is early evidence for AMG 757 clinical activity in SCLC (21), a tumor type reported to be enriched for immunosuppressive cells (33), pre-clinical and clinical studies have shown that BiTE® immune therapy upregulates the PD-1/PD-L1 immune checkpoint, which can limit efficacy. Measures to restore a more favorable anti-tumor immune microenvironment, including novel dosing strategies or checkpoint inhibitor combinations to prevent T cell dysfunction, will be important future areas to explore.

We developed a DLL3-targeting PET imaging agent to serve as a non-invasive biomarker of DLL3 expression. We envision that this diagnostic may help to identify patients who may respond to DLL3-targeted therapy. One potential use of DLL3 PET imaging would

be as a companion biomarker to DLL3-targeted therapeutics, an emerging strategy in drug development (34,35). For example, DLL3 PET scans could test for target expression and intertumoral heterogeneity, enabling more precision in patient selection and monitoring lesion-specific response and progression. Our imaging study demonstrates the specificity of [^{89}Zr]DFO-DLL3-scFv for DLL3-expressing tumors. Moreover, [^{89}Zr]DFO-DLL3-scFv was able to distinguish between low and high DLL3-expressing PDX tumors. Previously, the DLL3-targeting antibody SC16 was labeled with ^{89}Zr, and PET imaging was conducted in preclinical (36,37) and clinical (NCT04199741) studies. In contrast with the ^{89}Zr-labeled SC16 antibody, we utilized a scFv, which is smaller and yields more rapid target binding and clearance. This is a potential advantage that could enable same day or next-day imaging of patients, and better tumor penetration than a full-sized antibody. The high kidney uptake observed at early timepoints in our preclinical studies is expected based on the smaller size and renal clearance of scFv PET agents (38,39). Potential methods to improve the tumor signal to background ratio include optimizing different doses or timepoints, PEGylation of the targeting agent to increase the molecule size above the threshold for renal clearance (40), using alternative antibody formats such as diabodies or minibodies (41), or using enzymatic, brush border membrane cleavable linkers to reduce renal uptake of the antibody fragment (42). Further studies will need to be performed to elucidate the optimal antibody format for translational imaging studies (29). Overall, our data, in combination with prior studies (36,37), support further development of a DLL3-targeted PET imaging agent as a noninvasive diagnostic for DLL3-targeting therapeutics, and the development of potential radioimmunotherapy strategies to target DLL3-expressing tumors (43).

In conclusion, we demonstrate the first preclinical evidence showing robust AMG 757 anti-tumor activity in multiple clinically relevant *de novo* and treatment-emergent SCNC prostate cancer PDX models and the first radiographic objective response in a patient with SCNC prostate cancer treated with AMG 757. These data support the ongoing clinical trial evaluating AMG 757 activity in patients with this aggressive subtype of advanced prostate cancer (NCT04702737).

Supplementary Material

Refer to Web version on PubMed Central for supplementary material.

ACKNOWLEDGEMENTS:

JC is supported by a Young Investigator Award from the Prostate Cancer Foundation (20YOUN06) and the Department of Defense Physician's Research Award (W81XWH-20-1-0136).

RRF is supported by a Department of Defense Prostate Cancer Program Translational Science Award (W81XWH-20-1-0292)

FYF and AA are supported by the Benioff Initiative for Prostate Cancer Research at the University of California, San Francisco.

YW is supported by the Canadian Institutes of Health Research (#141635, #144159, #153081, #173338, #180554)

We thank Efrain Pacheco, Trish McElroy and Jinghui Zhan (Amgen, Inc.) for preclinical study support and the Preclinical Therapeutics Core at UCSF for technical support.

We thank the Prostate Cancer Foundation for funding support (to RRF, RA, ES, AA and FYF), our patients who participated in the PROMOTE biopsy clinical trial (NCT02735252) as well as our clinical research coordinators and staff.

Research reported in this publication was supported by the National Cancer Institute of the National Institutes of Health, and in part by the University of California, San Francisco Histology & Biomarker Core (HBC), under Award Number P30CA082103. The content is solely the responsibility of the authors and does not necessarily represent the official views of the National Institutes of Health.

DISCLOSURES STATEMENT:

AA is a co-founder of Tango Therapeutics, Azkarra Therapeutics, Ovibio Corporation, Kyttaro; a consultant for ProLynx, Cura, GenVivo; a member of the SAB of Genentech, GLAdiator, Circle, Cambridge Science Corporation, Bluestar, Phoenix Molecular Designs, Earli, Ambagon, GSK; receives grant/research support from SPARC and AstraZeneca; holds patents on the use of PARP inhibitors held jointly with AstraZeneca.

FYF has received consulting fees from Astellas, Bayer, Blue Earth Diagnostics, Celgene, Genentech, Janssen, Myovant, Roivant, and Sanofi.

RA has received research funding to the University of California, San Francisco from Janssen, Novartis, Amgen, Zenith Epigenetics, Merck, Cancer Targeted Technology, Xynomic Pharmaceuticals, AstraZeneca; and has received consulting fees from Dendreon, Pfizer, Jubilant Pharmaceuticals, AstraZeneca, Alessa Therapeutics, Advanced Accelerator Applications and Clovis Oncology.

JC has received consulting fees from Exai Bio.

FL, KSC, NHS, BY and JMB are employees of Amgen, Inc. MS is a former employee of Amgen, Inc.

This work received funding support by Amgen, Inc.

All other authors declare no potential conflicts of interest.

REFERENCES

1. Aggarwal R, Huang J, Alumkal JJ, Zhang L, Feng FY, Thomas GV, et al. Clinical and Genomic Characterization of Treatment-Emergent Small-Cell Neuroendocrine Prostate Cancer: A Multi-institutional Prospective Study. J Clin Oncol 2018;36(24):2492–503 doi 10.1200/JCO.2017.77.6880. [PubMed: 29985747]
2. Spetsieris N, Boukovala M, Patsakis G, Alafis I, Efstathiou E. Neuroendocrine and Aggressive-Variant Prostate Cancer. Cancers (Basel) 2020;12(12) doi 10.3390/cancers12123792.
3. Aparicio AM, Harzstark AL, Corn PG, Wen S, Araujo JC, Tu SM, et al. Platinum-based chemotherapy for variant castrate-resistant prostate cancer. Clin Cancer Res 2013;19(13):3621–30 doi 10.1158/1078-0432.CCR-12-3791. [PubMed: 23649003]
4. Chapman G, Sparrow DB, Kremmer E, Dunwoodie SL. Notch inhibition by the ligand DELTA-LIKE 3 defines the mechanism of abnormal vertebral segmentation in spondylocostal dysostosis. Hum Mol Genet 2011;20(5):905–16 doi 10.1093/hmg/ddq529. [PubMed: 21147753]
5. Dunwoodie SL, Clements M, Sparrow DB, Sa X, Conlon RA, Beddington RS. Axial skeletal defects caused by mutation in the spondylocostal dysplasia/pudgy gene Dll3 are associated with disruption of the segmentation clock within the presomitic mesoderm. Development 2002;129(7):1795–806. [PubMed: 11923214]
6. Bulman MP, Kusumi K, Frayling TM, McKeown C, Garrett C, Lander ES, et al. Mutations in the human delta homologue, DLL3, cause axial skeletal defects in spondylocostal dysostosis. Nat Genet 2000;24(4):438–41 doi 10.1038/74307. [PubMed: 10742114]
7. Ladi E, Nichols JT, Ge W, Miyamoto A, Yao C, Yang LT, et al. The divergent DSL ligand Dll3 does not activate Notch signaling but cell autonomously attenuates signaling induced by other DSL ligands. J Cell Biol 2005;170(6):983–92 doi 10.1083/jcb.200503113. [PubMed: 16144902]
8. Saunders LR, Bankovich AJ, Anderson WC, Aujay MA, Bheddah S, Black K, et al. A DLL3-targeted antibody-drug conjugate eradicates high-grade pulmonary neuroendocrine tumor-initiating cells in vivo. Sci Transl Med 2015;7(302):302ra136 doi 10.1126/scitranslmed.aac9459.

9. Rudin CM, Pietanza MC, Bauer TM, Ready N, Morgensztern D, Glisson BS, et al. Rovalpituzumab tesirine, a DLL3-targeted antibody-drug conjugate, in recurrent small-cell lung cancer: a first-in-human, first-in-class, open-label, phase 1 study. Lancet Oncol 2017;18(1):42–51 doi 10.1016/S1470-2045(16)30565-4. [PubMed: 27932068]
10. Blackhall F, Jao K, Greillier L, Cho BC, Penkov K, Reguart N, et al. Efficacy and Safety of Rovalpituzumab Tesirine Compared With Topotecan as Second-Line Therapy in DLL3-High SCLC: Results From the Phase 3 TAHOE Study. J Thorac Oncol 2021;16(9):1547–58 doi 10.1016/j.jtho.2021.02.009. [PubMed: 33607312]
11. Mansfield AS, Hong DS, Hann CL, Farago AF, Beltran H, Waqar SN, et al. A phase I/II study of rovalpituzumab tesirine in delta-like 3-expressing advanced solid tumors. NPJ Precis Oncol 2021;5(1):74 doi 10.1038/s41698-021-00214-y. [PubMed: 34354225]
12. Johnson ML, Zvirbule Z, Laktionov K, Helland A, Cho BC, Gutierrez V, et al. Rovalpituzumab Tesirine as a Maintenance Therapy After First-Line Platinum-Based Chemotherapy in Patients With Extensive-Stage-SCLC: Results From the Phase 3 MERU Study. J Thorac Oncol 2021;16(9):1570–81 doi 10.1016/j.jtho.2021.03.012. [PubMed: 33823285]
13. Hann CL, Burns TF, Dowlati A, Morgensztern D, Ward PJ, Koch MM, et al. A Phase 1 Study Evaluating Rovalpituzumab Tesirine in Frontline Treatment of Patients With Extensive-Stage SCLC. J Thorac Oncol 2021;16(9):1582–8 doi 10.1016/j.jtho.2021.06.022. [PubMed: 34242790]
14. Malhotra J, Nikolinakos P, Leal T, Lehman J, Morgensztern D, Patel JD, et al. A Phase 1–2 Study of Rovalpituzumab Tesirine in Combination With Nivolumab Plus or Minus Ipilimumab in Patients With Previously Treated Extensive-Stage SCLC. J Thorac Oncol 2021;16(9):1559–69 doi 10.1016/j.jtho.2021.02.022. [PubMed: 33652156]
15. Uprety D, Remon J, Adjei AA. All That Glitters Is Not Gold: The Story of Rovalpituzumab Tesirine in SCLC. J Thorac Oncol 2021;16(9):1429–33 doi 10.1016/j.jtho.2021.07.012. [PubMed: 34425994]
16. Miller ML, Shizuka M, Wilhelm A, Salomon P, Reid EE, Lanieri L, et al. A DNA-Interacting Payload Designed to Eliminate Cross-Linking Improves the Therapeutic Index of Antibody-Drug Conjugates (ADCs). Mol Cancer Ther 2018;17(3):650–60 doi 10.1158/1535-7163.MCT-17-0940. [PubMed: 29440292]
17. Puca L, Gavyert K, Sailer V, Conteduca V, Dardenne E, Sigouros M, et al. Delta-like protein 3 expression and therapeutic targeting in neuroendocrine prostate cancer. Sci Transl Med 2019;11(484) doi 10.1126/scitranslmed.aav0891.
18. Owen DH, Giffin MJ, Bailis JM, Smit MD, Carbone DP, He K. DLL3: an emerging target in small cell lung cancer. J Hematol Oncol 2019;12(1):61 doi 10.1186/s13045-019-0745-2. [PubMed: 31215500]
19. Goebeler ME, Bargou RC. T cell-engaging therapies - BiTEs and beyond. Nat Rev Clin Oncol 2020;17(7):418–34 doi 10.1038/s41571-020-0347-5. [PubMed: 32242094]
20. Giffin MJ, Cooke K, Lobenhofer EK, Estrada J, Zhan J, Deegen P, et al. AMG 757, a Half-Life Extended, DLL3-Targeted Bispecific T-Cell Engager, Shows High Potency and Sensitivity in Preclinical Models of Small-Cell Lung Cancer. Clin Cancer Res 2021;27(5):1526–37 doi 10.1158/1078-0432.CCR-20-2845. [PubMed: 33203642]
21. Owonikoko TK, Champiat S, Johnson ML, Govindan R, Izumi H, Lai WVV, et al. Updated results from a phase 1 study of AMG 757, a half-life extended bispecific T-cell engager (BiTE) immuno-oncology therapy against delta-like ligand 3 (DLL3), in small cell lung cancer (SCLC). Journal of Clinical Oncology 2021;39(15_suppl):8510- doi 10.1200/JCO.2021.39.15_suppl.8510.
22. Borghaei H, Paz-Ares L, Johnson M, Champiat S, Owonikoko TK, Lai V, et al. Phase 1 Updated Exploration and First Expansion Data for DLL3-Targeted T-cell Engager Tarlatamab in SCLC (DeLLphi-300 Study). IASLC World Conference on Lung Cancer 2022.
23. Shi M, Wang Y, Lin D, Wang Y. Patient-derived xenograft models of neuroendocrine prostate cancer. Cancer Lett 2022;525:160–9 doi 10.1016/j.canlet.2021.11.004. [PubMed: 34767925]
24. Quigley DA, Dang HX, Zhao SG, Lloyd P, Aggarwal R, Alumkal JJ, et al. Genomic Hallmarks and Structural Variation in Metastatic Prostate Cancer. Cell 2018;175(3):889 doi 10.1016/j.cell.2018.10.019. [PubMed: 30340047]

25. Lin D, Wyatt AW, Xue H, Wang Y, Dong X, Haegert A, et al. High fidelity patient-derived xenografts for accelerating prostate cancer discovery and drug development. Cancer Res 2014;74(4):1272–83 doi 10.1158/0008-5472.CAN-13-2921-T. [PubMed: 24356420]
26. Wang S, Li J, Hua J, Su Y, Beckford-Vera DR, Zhao W, et al. Molecular Imaging of Prostate Cancer Targeting CD46 Using ImmunoPET. Clin Cancer Res 2021;27(5):1305–15 doi 10.1158/1078-0432.CCR-20-3310. [PubMed: 33293372]
27. Beltran H, Prandi D, Mosquera JM, Benelli M, Puca L, Cyrta J, et al. Divergent clonal evolution of castration-resistant neuroendocrine prostate cancer. Nat Med 2016;22(3):298–305 doi 10.1038/nm.4045. [PubMed: 26855148]
28. Sharma SK, Lyashchenko SK, Park HA, Pillarsetty N, Roux Y, Wu J, et al. A rapid bead-based radioligand binding assay for the determination of target-binding fraction and quality control of radiopharmaceuticals. Nucl Med Biol 2019;71:32–8 doi 10.1016/j.nucmedbio.2019.04.005. [PubMed: 31128476]
29. Knowles SM, Wu AM. Advances in immuno-positron emission tomography: antibodies for molecular imaging in oncology. J Clin Oncol 2012;30(31):3884–92 doi 10.1200/JCO.2012.42.4887. [PubMed: 22987087]
30. Cejas P, Xie Y, Font-Tello A, Lim K, Syamala S, Qiu X, et al. Subtype heterogeneity and epigenetic convergence in neuroendocrine prostate cancer. Nat Commun 2021;12(1):5775 doi 10.1038/s41467-021-26042-z. [PubMed: 34599169]
31. Gay CM, Stewart CA, Park EM, Diao L, Groves SM, Heeke S, et al. Patterns of transcription factor programs and immune pathway activation define four major subtypes of SCLC with distinct therapeutic vulnerabilities. Cancer Cell 2021;39(3):346–60 e7 doi 10.1016/j.ccell.2020.12.014. [PubMed: 33482121]
32. Henke RM, Meredith DM, Borromeo MD, Savage TK, Johnson JE. Ascl1 and Neurog2 form novel complexes and regulate Delta-like3 (Dll3) expression in the neural tube. Dev Biol 2009;328(2):529–40 doi 10.1016/j.ydbio.2009.01.007. [PubMed: 19389376]
33. Chan JM, Quintanal-Villalonga A, Gao VR, Xie Y, Allaj V, Chaudhary O, et al. Signatures of plasticity, metastasis, and immunosuppression in an atlas of human small cell lung cancer. Cancer Cell 2021;39(11):1479–96 e18 doi 10.1016/j.ccell.2021.09.008. [PubMed: 34653364]
34. Carmon KS, Azhdarinia A. Application of Immuno-PET in Antibody-Drug Conjugate Development. Mol Imaging 2018;17:1536012118801223 doi 10.1177/1536012118801223.
35. McKnight BN, Viola-Villegas NT. (89) Zr-ImmunoPET companion diagnostics and their impact in clinical drug development. J Labelled Comp Radiopharm 2018;61(9):727–38 doi 10.1002/jlcr.3605. [PubMed: 29341222]
36. Sharma SK, Pourat J, Abdel-Atti D, Carlin SD, Piersigilli A, Bankovich AJ, et al. Noninvasive Interrogation of DLL3 Expression in Metastatic Small Cell Lung Cancer. Cancer Res 2017;77(14):3931–41 doi 10.1158/0008-5472.CAN-17-0299. [PubMed: 28487384]
37. Korsen JA, Kalidindi TM, Khitrov S, Samuels ZV, Chakraborty G, Gutierrez JA, et al. Molecular imaging of Neuroendocrine Prostate Cancer by targeting Delta-like Ligand 3. J Nucl Med 2022 doi 10.2967/jnumed.121.263221.
38. He J, Wang Y, Feng J, Zhu X, Lan X, Iyer AK, et al. Targeting prostate cancer cells in vivo using a rapidly internalizing novel human single-chain antibody fragment. J Nucl Med 2010;51(3):427–32 doi 10.2967/jnumed.109.069492. [PubMed: 20150269]
39. Mukai H, Watanabe Y. Review: PET imaging with macro- and middle-sized molecular probes. Nucl Med Biol 2021;92:156–70 doi 10.1016/j.nucmedbio.2020.06.007. [PubMed: 32660789]
40. Scott AM, Akhurst T, Lee FT, Ciprotti M, Davis ID, Weickhardt AJ, et al. First clinical study of a pegylated diabody (124)I-labeled PEG-AVP0458 in patients with tumor-associated glycoprotein 72 positive cancers. Theranostics 2020;10(25):11404–15 doi 10.7150/thno.49422. [PubMed: 33052222]
41. Wu AM, Pandit-Taskar N. ImmunoPET: harnessing antibodies for imaging immune cells. Mol Imaging Biol 2022;24(2):181–97 doi 10.1007/s11307-021-01652-7. [PubMed: 34550529]
42. Suzuki C, Uehara T, Kanazawa N, Wada S, Suzuki H, Arano Y. Preferential Cleavage of a Tripeptide Linkage by Enzymes on Renal Brush Border Membrane To Reduce Renal Radioactivity

Levels of Radiolabeled Antibody Fragments. J Med Chem 2018;61(12):5257–68 doi 10.1021/acs.jmedchem.8b00198. [PubMed: 29869881]

43. Tully KM, Tendler S, Carter LM, Sharma SK, Samuels ZV, Mandleywala K, et al. Radioimmunotherapy Targeting Delta-like Ligand 3 in Small Cell Lung Cancer Exhibits Antitumor Efficacy with Low Toxicity. Clin Cancer Res 2022;28(7):1391–401 doi 10.1158/1078-0432.CCR-21-1533. [PubMed: 35046060]

STATEMENT OF SIGNIFICANCE:

The preclinical and clinical evaluation of DLL3-directed immunotherapy, AMG 757, and development of a PET radiotracer for noninvasive DLL3 detection demonstrate the potential of targeting DLL3 in small cell neuroendocrine prostate cancer.

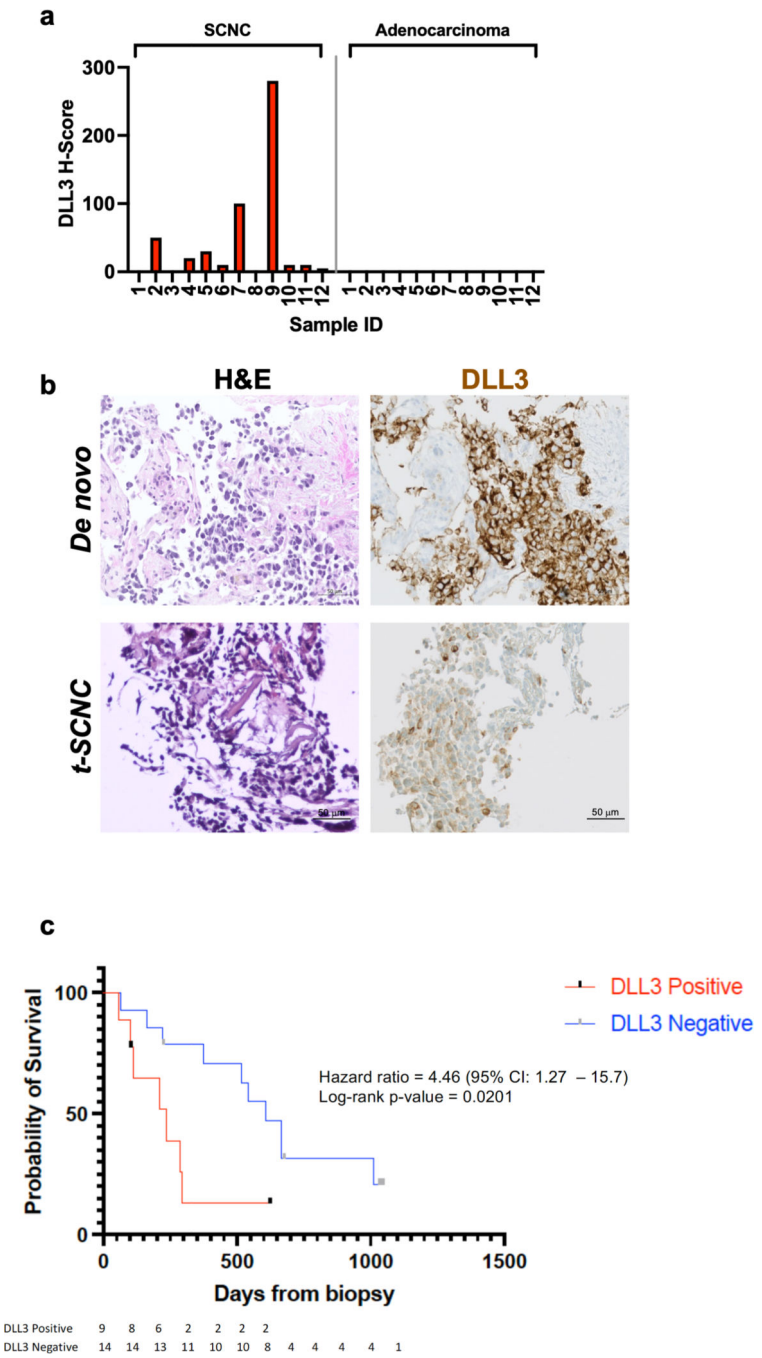

Figure 1. DLL3 Expression by Histologic Subtype of mCRPC.

a. DLL3 expression by H-score across samples with *de novo* and t-SCNC (n = 12) versus adenocarcinoma (n = 12) histologic differentiation. **b.** H&E and IHC stains for DLL3 in *de novo* and t-SCNC biopsies. Scale bar, 50 μM. **c.** Overall survival from date of biopsy for patients harboring mCRPC biopsies that were positive vs. negative for DLL3 expression. (HR = hazard ratio; CI = confidence interval). The number at risk for each group is indicated and censored data are indicated by the gray tick marks.

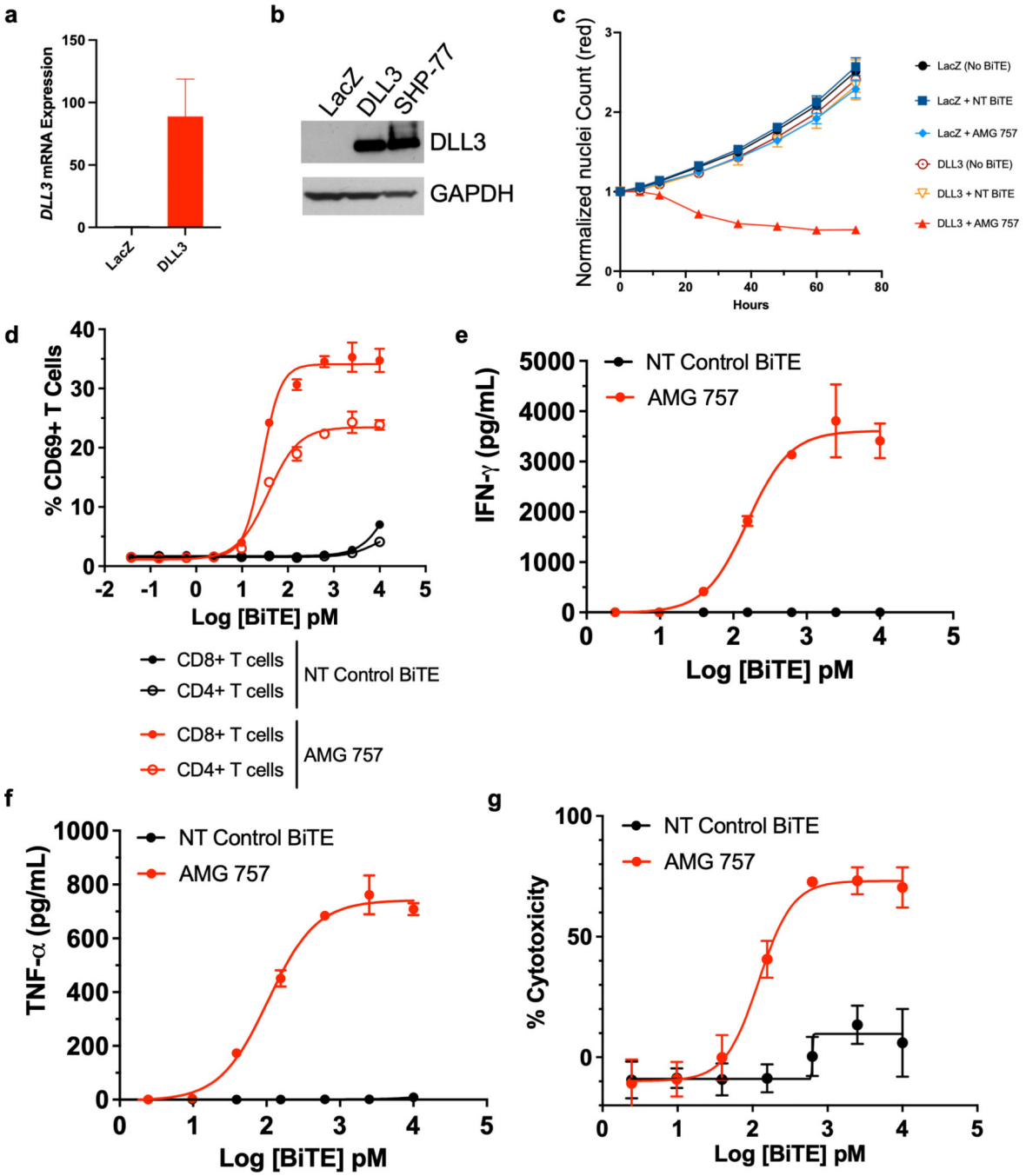

Figure 2. AMG 757 Activity Against DLL3-expressing Prostate Cancer Cells *in vitro*.

a. Relative *DLL3* mRNA expression in 22RV1 prostate cancer cells expressing LacZ (control) or DLL3. **b.** Western blot showing DLL3 protein expression in 22RV1 cells expressing LacZ (control) or DLL3. SCLC SHP-77 cells were used as a positive control. GAPDH is shown as loading control. **c.** Growth curves normalized by nuclei count (NucLightRed) in 22RV1-LacZ and 22RV1-DLL3 cells co-cultured with human T cells and treated with a NT control BiTE® molecule or AMG 757. **d-g.** Co-cultures of NCI-H660 prostate cancer cells with human T cells and AMG 757 (red) or a NT control BiTE molecule

(black) were assayed for **d.** CD69 activation of CD4+ and CD8+ T cells; **e-f.** IFNγ (e) and TNFα (f) secretion; **g.** cytotoxicity of NCI-H660 cells.

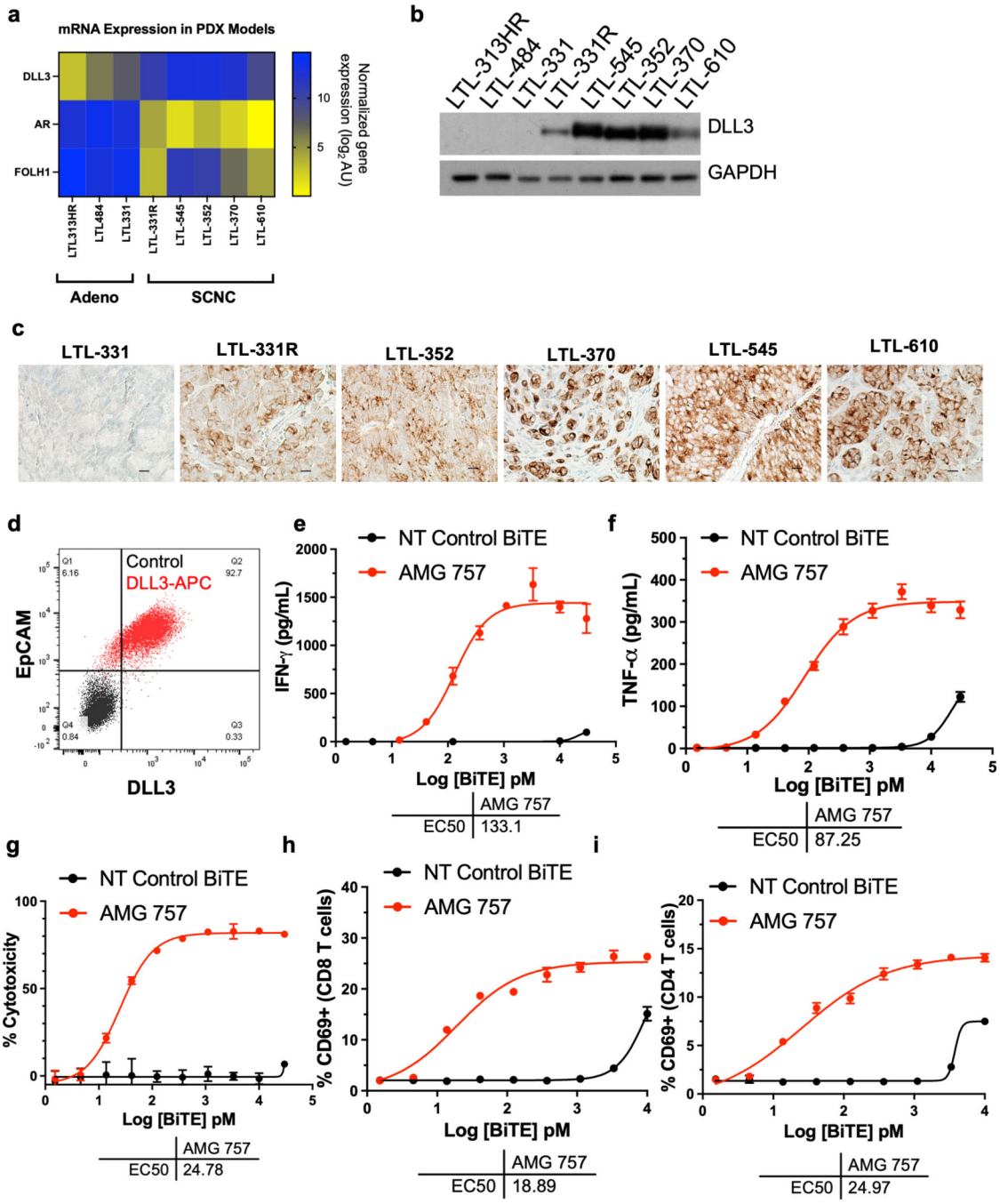

Figure 3. DLL3 Expression and AMG 757 Activity in Prostate PDX Tumor Cells.

a. mRNA expression of *DLL3, AR* and *FOLH1* across 3 prostate cancer adenocarcinoma and 5 prostate cancer SCNC lines, including one t-SCNC line (LTL-331R). mRNA expression is normalized gene expression (log2) arbitrary units (AU). **b.** Western blot showing DLL3 expression in the PDX cell lines. **c.** DLL3 expression by IHC in the models indicated. Scale bar, 50 μM. **d.** Scatter plot showing DLL3 expression in dissociated tumor cells from the LTL-331R PDX line. Cells stained with a nontargeting antibody as a control are shown in black (Control). Cells stained with an anti-EpCAM antibody conjugated to

FITC and anti-DLL3 antibody conjugated to APC are shown in red. **e-i.** Co-cultures of LTL-331R PDX cells with human T cells were incubated with AMG 757 (red) or NT control BiTE molecule (black) and assayed for **e.** IFNγ; **f.** TNFα; **g.** LTL-331R tumor cell cytotoxicity; **h.** activation of CD8+ T cells; and **i.** activation of CD8+ T cells. The AMG 757 EC_{50} is shown for each assay.

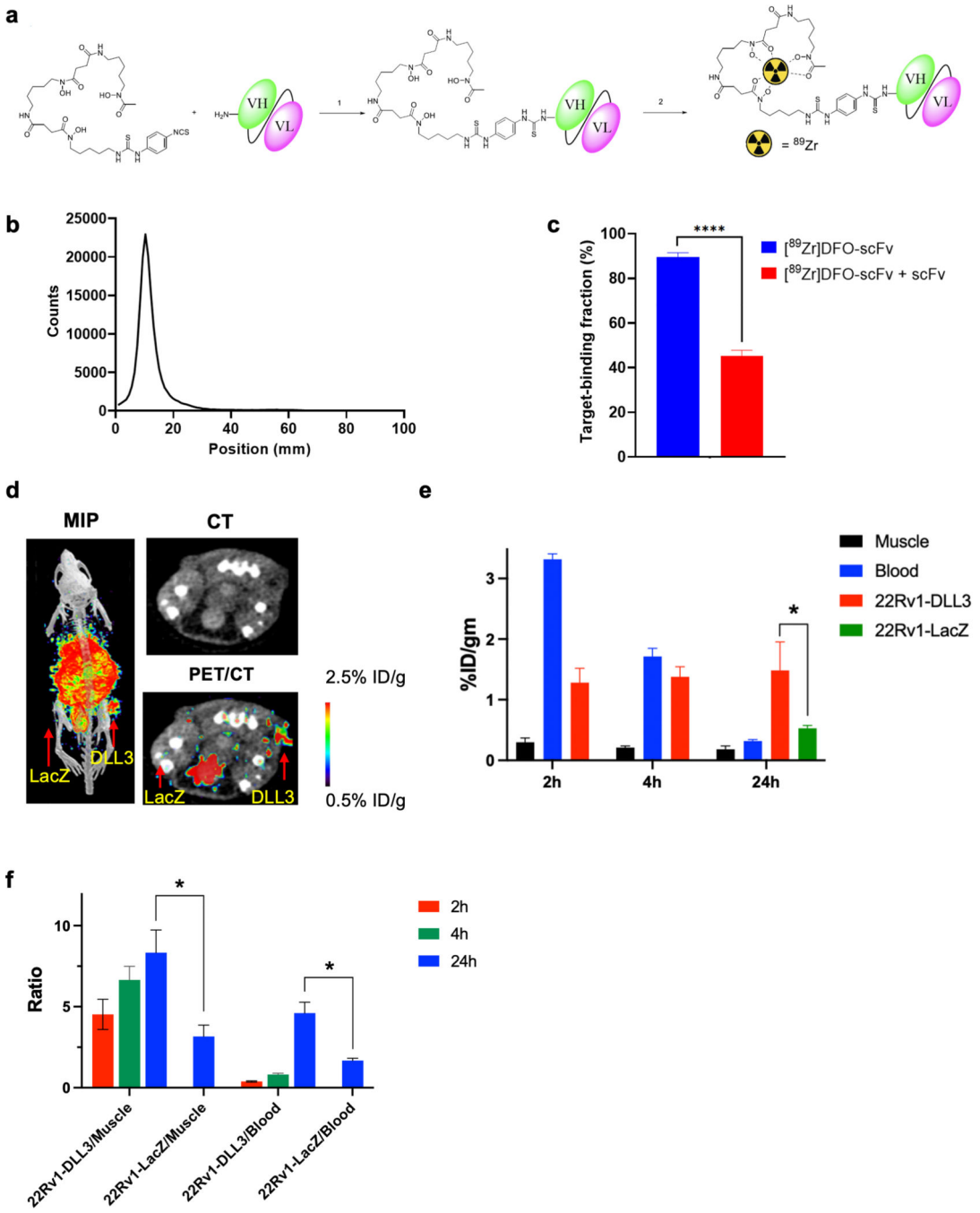

Figure 4. [^{89}Zr]DFO-DLL3-scFv ImmunoPET Imaging of DLL3+ Tumor Xenografts.

a. Schematic for [^{89}Zr]DFO-scFv generation. **b.** iTLC analysis of purified [^{89}Zr]DFO-scFv. **c.** Magnetic bead–based radioligand binding assay for DLL3 target binding fraction in the absence or presence of unlabeled DLL3 scFv. **** $p < 0.0001$. **d.** Maximum-intensity projection (MIP) μPET/CT, transaxial CT, and transaxial μPET/CT slices obtained 24h after administration of [^{89}Zr]DFO-scFv in 22RV1-LacZ and 22RV1-DLL3 dual tumor xenografts. **e.** Biodistribution data of [^{89}Zr]DFO-scFv from selected tissues from 2h to 24h in mice bearing 22Rv1-LacZ and 22RV1-DLL3 dual tumors. **f.** Tumor/blood and tumor/muscle ratio

of [^{89}Zr]DFO-scFv from 2h to 24h in 22Rv1-LacZ and 22RV1-DLL3 dual tumors. *p < 0.05.

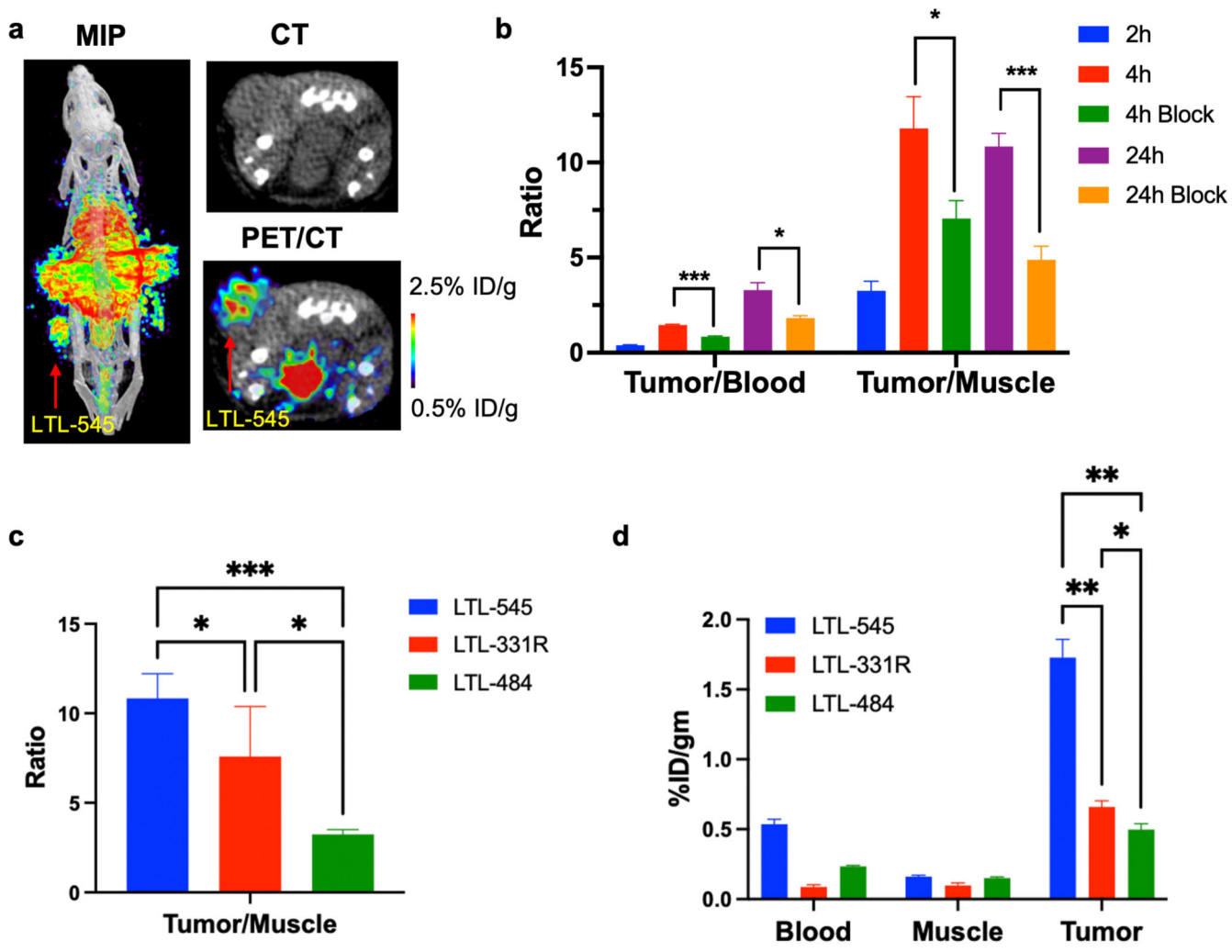

Figure 5. DLL3 ImmunoPET Imaging Across Multiple PDX Models.

a. Maximum-intensity projection (MIP) μPET/CT, transaxial CT, and transaxial μPET/CT slices obtained 24h after administration of [^{89}Zr]DFO-scFv in mice bearing LTL-545 PDX tumors. **b.** Tumor/blood and tumor/muscle ratio of [^{89}Zr]DFO-DLL3-scFv (with scFv block) at 2h, 4h, and 24h in mice bearing LTL-545 PDX xenografts. ns= not significant, * $p < 0.05$, *** $p < 0.001$. **c.** Tumor/blood and tumor/muscle ratio of [^{89}Zr]DFO-DLL3-scFv in LTL-545 (DLL3^{HI}), LTL-331R (DLL3^{LOW}) and LTL-484 (DLL3^{NEGATIVE}) models at 24h post-injection. * $p< 0.05$, *** $p < 0.001$. **d.** Biodistribution data of [^{89}Zr]DFO-scFv from selected tissues in LTL-545, LTL-331R and LTL-484 models at 24h post-injection.

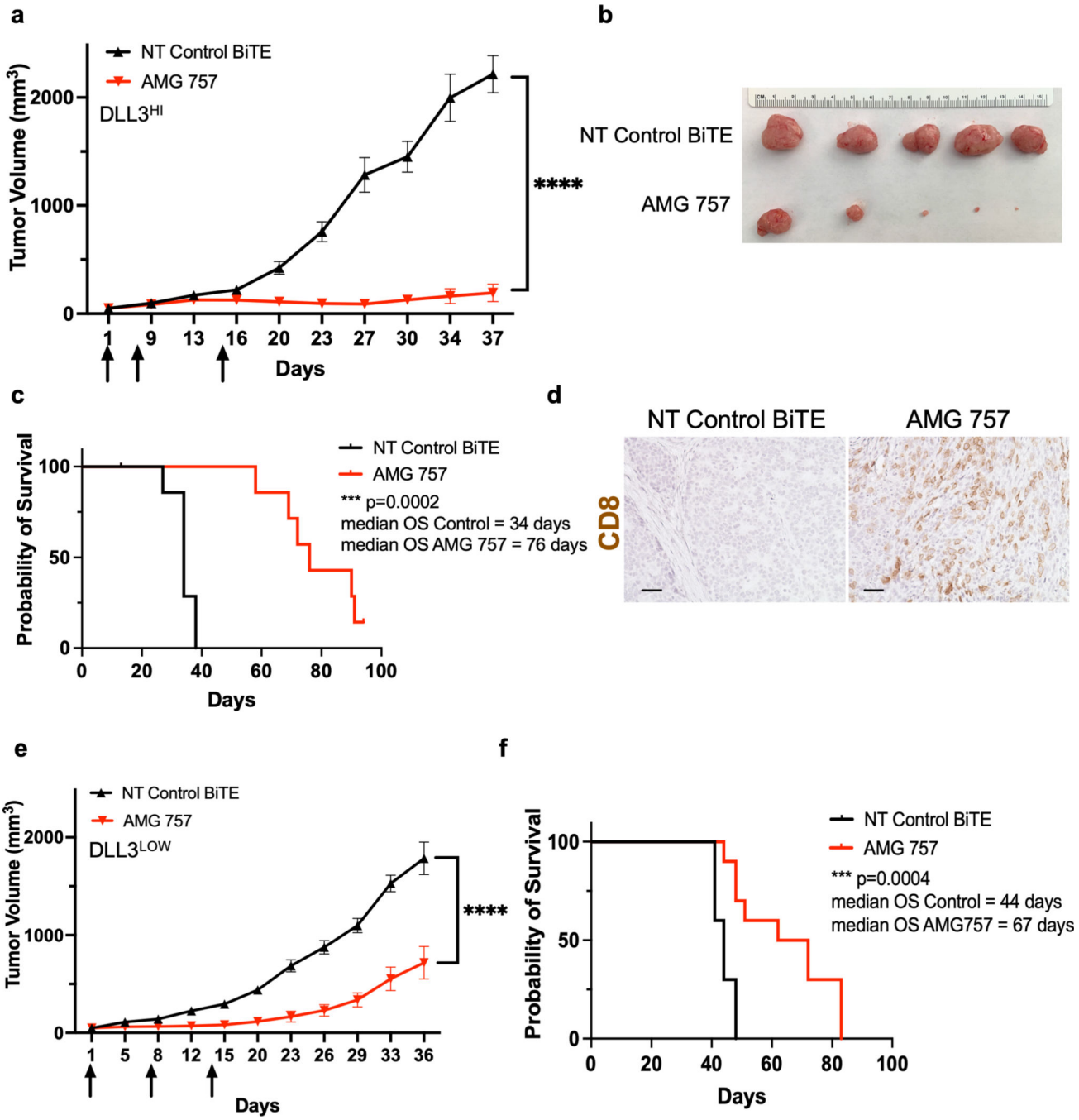

Figure 6. AMG 757 Antitumor Activity in DLL^{HI} and DLL3^{LOW} PDX Models.

a. Tumor growth curves in mice bearing LTL-545 PDX tumors (**DLL^{HI}**) treated with AMG 757 (red) or NT Control BiTE® (black). Mice were administered human T cells on Day 0. Arrows indicate days of BiTE® treatment. **b.** Images of the endpoint tumors from mice in the study shown in **(a). c.** Kaplan-Meier survival curve of mice in the study shown in **(a).** Median OS is shown, n=15 mice per group. **d.** IHC images of CD8+ T cells in LTL-545 tumors taken 5 days after the first AMG 757 or NT control BiTE® treatment in **(a)**. Scale bar, 50 μM. **e.** Tumor growth curves in mice bearing LTL-331R PDX tumors (**DLL3^{LOW}**)

treated with AMG 757 (red) or NT control BiTE® (black). **f.** Kaplan-Meier survival curve of mice from the study shown in **(e)**. Median OS is shown, n = 10 mice per group. No mice were censored for panels c and f.

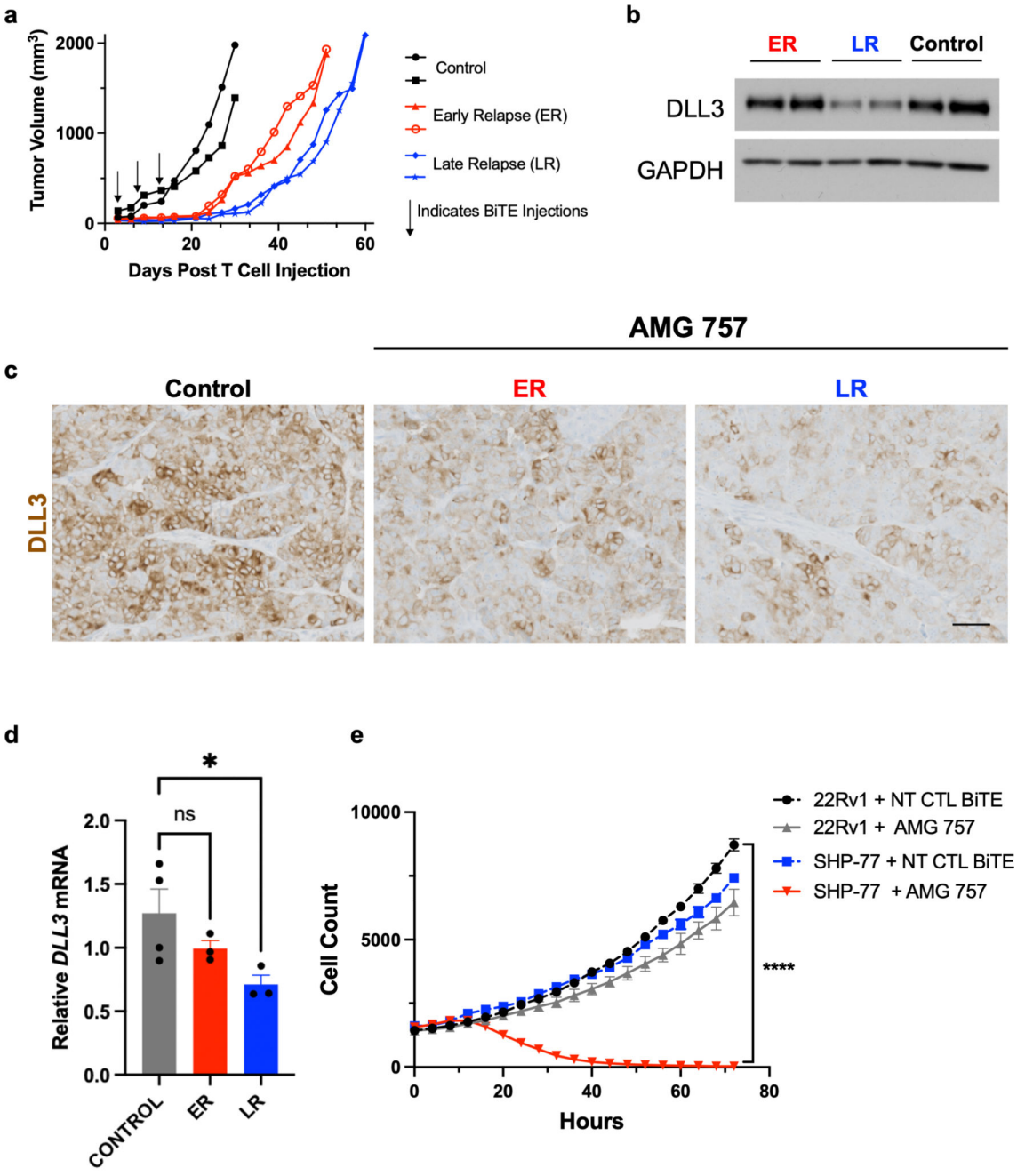

Figure 7. DLL3 Expression in Relapsed LTL-331R Tumors.

a. Individual tumor growth curves in mice bearing LTL-331R PDX tumors treated with AMG 757 or NT Control (CTL) BiTE®. Mice that received AMG 757 showed early relapse (ER, red) or late relapse (LR, blue). **b.** Western blot for DLL3 expression in control or relapsed tumor samples. **c.** IHC showing DLL3 expression in control or relapsed tumor samples. Scale bar, 100 μM. **d.** DLL3 mRNA expression in control or relapsed tumor samples by qPCR. * $p<0.05$. **e.** 22RV1 (labeled with NucLightGreen) and SHP-77 (labeled with NucLightRed) cells were mixed at a 1:1 ratio, and co-cultured with T cells. For each

condition, the number of 22RV1 and SHP-77 cells in the presence of either NT CTL BiTE® or AMG 757 is shown and plotted over time. **** $p<0.0001$ for cell count at the final time point, between SHP-77 + AMG 757 vs all other conditions.

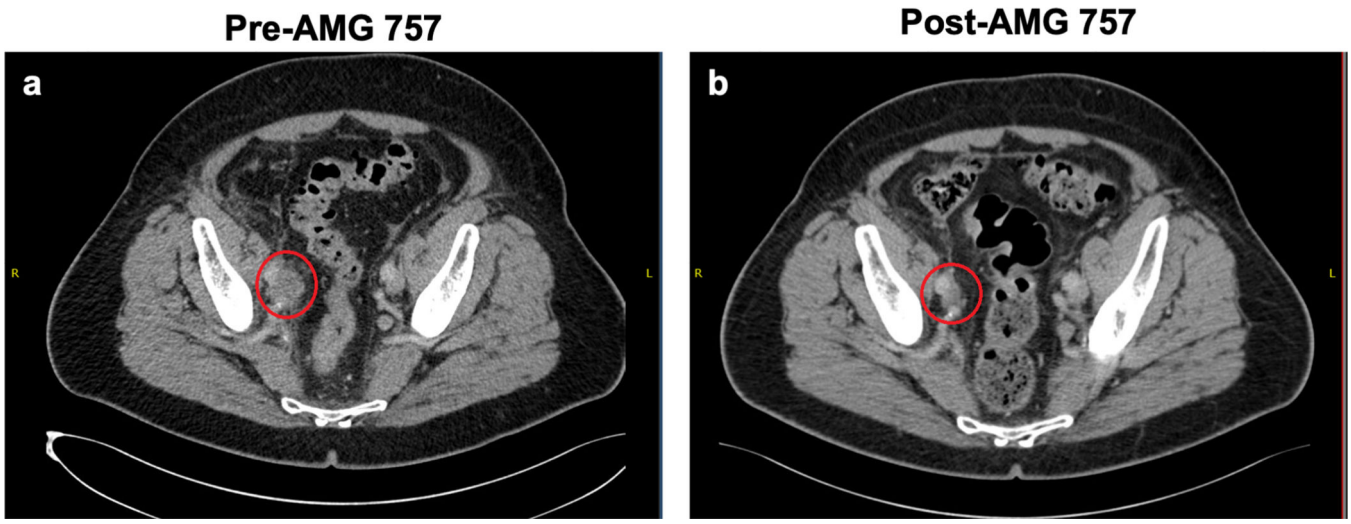

Figure 8. Confirmed Objective Response in a Patient with Histologically-Confirmed SCNC Treated with AMG 757.

a. Computed tomography (CT) scan before AMG 757 therapy showing the patient's right pelvic soft tissue mass, indicated by the red circle, and significant right-sided hydronephrosis. **b.** CT scan of the patient's pelvis after 15 weeks on AMG 757 therapy shows a partial response by RECIST criteria (greater than 30% reduction in size) and near resolution of the right-sided hydronephrosis.